Targeted radionuclide therapy in patient-derived xenografts using ^{177}Lu-EB-RGD

Liang Zhao[1,*], Haojun Chen[2,*], Zhide Guo[3,*], Kaili Fu[1], Lanling Yao[2], Li Fu[4], Weixi Guo[5], Xuejun Wen[3], Orit Jacobson[6], Xianzhong Zhang[3], Long Sun[2], Hua Wu[2], Qin Lin[1], Xiaoyuan Chen[6]

[1]Department of Radiation Oncology, Xiamen Cancer Hospital, The First Affiliated Hospital of Xiamen University, Xiamen, China

[2]Department of Nuclear Medicine and Minnan PET Center, Xiamen Cancer Hospital, The First Affiliated Hospital of Xiamen University, Xiamen, China

[3]State Key Laboratory of Molecular Vaccinology and Molecular Diagnostics & Center for Molecular Imaging and Translational Medicine, School of Public Health, Xiamen University, Xiamen, China

[4]Department of Pathology, Xiamen Cancer Hospital, The First Affiliated Hospital of Xiamen University, Xiamen, China

[5]Department of Thoracic Surgery, Xiamen Cancer Hospital, The First Affiliated Hospital of Xiamen University, Xiamen, China

[6]Laboratory of Molecular Imaging and Nanomedicine, National Institute of Biomedical Imaging and Bioengineering, National Institutes of Health, Bethesda, Maryland, USA

Abstract

Currently, most patients with non-small cell lung cancer (NSCLC) are diagnosed in advanced stages with a poor five-year survival rate. Therefore, intensive research aimed at finding novel therapeutic strategies has been ongoing; experimental models that reliably emulate NSCLC

Corresponding authors: Haojun Chen, MD, PhD, Department of Nuclear Medicine and Minnan PET Center, Xiamen Cancer Hospital, The First Affiliated Hospital of Xiamen University, Xiamen 361003, China. Tel: +86-592-2137077. leochen0821@foxmail.com, Qin Lin, MD, PhD, Department of Radiation Oncology, Xiamen Cancer Hospital, The First Affiliated Hospital of Xiamen University, Xiamen 361003, China. Tel: +86-592-2139152. linqin05@163.com, Xiaoyuan Chen, PhD, Laboratory of Molecular Imaging and Nanomedicine, National Institute of Biomedical Imaging and Bioengineering, National Institutes of Health, Bethesda, MD 20814, USA. Tel: +1-3013267145. shawn.chen@nih.gov.
[*]These authors contributed equally to this work.

disease are greatly needed to predict responses to novel therapeutics. Therefore, we developed patient-derived xenograft models of NSCLC, which we then used to evaluate the therapeutic efficacy of ^{177}Lu-EB-RGD, a peptide-based radiopharmaceutical with improved pharmacokinetics that targets integrin $\alpha_v\beta_3$. In this study, three different groups of NSCLC-PDXs were successfully established, all of which maintained the same immunohistochemical and genetic characteristics of the human primary tumour. The two NSCLC-PDX groups with intense and low expression of integrin $\alpha_v\beta_3$ (denoted as $PDX_{\alpha v\beta3+}$ and $PDX_{\alpha v\beta3-}$) were chosen as the experimental models to evaluate the *in vivo* biological behaviour of ^{177}Lu-EB-RGD. In SPECT imaging and biodistribution studies, ^{177}Lu-EB-RGD showed significantly higher accumulation in $PDX_{\alpha v\beta3+}$ and $PDX_{\alpha v\beta3-}$ models than its corresponding monomer ^{177}Lu-RGD. A single dose of 18.5 MBq ^{177}Lu-EB-RGD was enough to completely eradicate the tumours in $PDX_{\alpha v\beta3+}$, with no sign of tumour recurrence during the observation period. Such treatment was also efficacious in $PDX_{\alpha v\beta3-}$: a single dose of 29.6 MBq ^{177}Lu-EB-RGD led to a significant delay in tumour growth as compared to that in the control or ^{177}Lu-RGD group. The preclinical data from the use of this model suggest that ^{177}Lu- EB-RGD may be an effective treatment option for NSCLC and should be further evaluated in human trials.

Keywords

Non-small cell lung cancer; targeted radionuclide therapy; patient derived xenograft; ^{177}Lu-EB-RGD

Introduction

Lung cancer is the leading cause of cancer-related death worldwide; approximately 2 million new cases and 1.8 million deaths were reported in 2018 by Global Cancer Statistics 2018[1]. The two major forms of lung cancer are non-small cell lung cancer (NSCLC) and small cell lung cancer (SCLC). NSCLC accounts for approximately 80–85% of lung cancers, and adenocarcinoma is the most common histological subtype. Currently, most NSCLC patients are diagnosed in advanced stages with five-year survival rates of less than 10%[2]. Chemotherapy based on platinum is the first-line treatment for NSCLC but only provides a modest survival benefit[3]. Therefore, a better understanding of the molecular basis of the NSCLC and novel therapies are needed to significantly improve patient outcome.

The last decade has witnessed a paradigm shift from cytotoxic drugs to targeted therapy in medical oncology and pharmaceutical innovation. Inspired by breakthroughs in molecular and cellular biology, several novel synthesised chemical compounds and recombinant antibodies have been developed to selectively target oncogenic signalling pathways in NSCLC[4]. Such targeted therapeutic agents show impressive clinical efficacy and often significantly prolong the overall survival of individuals with NSCLC. Inevitably, however, the treated tumours recur as resistance to these targeted therapies develops[5]. More recently, immunotherapies such as PD-1/PD-L1 immune checkpoint blockades (ICB) have shown promise, with their durable response in advanced NSCLC without driver oncogene mutations[6]. However, the low objective response rate is the main obstruction to using ICBs more widely.

Targeted radionuclide therapy (TRT), a branch of radiotherapy, uses isotope emitting charged particles after labelling with a targeting vector. A carrier molecule can seek special molecular or functional targets. Besides being utilised in the treatment of local tumours like external radiotherapy, TRT can treat metastatic tumours through systemic administration[7]. A unique feature of radionuclides is that they can exert the "cross-fire" effect, potentially destroying adjacent tumour cells[8]. On January of 2018, ^{177}Lu-labelled dodecanetetraacetic acid tyrosine-3-octreotate (DOTATATE) (trade name Lutathera) was approved by the FDA to treat patients with somatostatin receptor-positive gastroenteropancreatic neuroendocrine tumours (NETs)[9].

Patient-derived xenografts (PDXs), obtained by direct implantation of tissue fragments into immunodeficient mice, are of particular interest because they retain the morphology, architecture, and molecular signatures of the corresponding parental tumour more closely than is possible for *in vitro* established cell lines. PDXs have been successfully investigated to identify specific determinants of therapeutic response and to predict the therapy response of individual tumours to chemotherapy and targeted therapy. However, the potential of PDXs to predict the response of NSCLC to TRT has not been investigated. This has important clinical implications for patients with advanced NSCLC, especially for those who are ineffective or resistant to platinum-based therapy or epidermal growth factor receptor-tyrosine kinase inhibitors. In the present study, we investigated the therapeutic efficacy of peptide-based TRT in PDXs derived from NSCLC. The Arg-Gly-Asp (RGD) peptide targets the integrin $\alpha_v\beta_3$ receptor on the tumour cells and neovasculature, which is highly expressed in many cancers[10]. Our previous investigation has demonstrated the positive expression of integrin $\alpha_v\beta_3$ in patients with NSCLC and ^{68}Ga labelled RGD peptide (^{68}Ga-NOTA-PRGD2) could be of use for lesion detection and help stage patients with NSCLC[11]. In this research, RGD was chemically conjugated with an albumin-binding moiety—truncated Evans Blue (denoted as EB-RGD). The major feature was the inclusion of the EB-derived albumin-binding moiety that affected the pharmacokinetics in a positive manner to elevate tumour uptake and tumour residence time[12,13]. For TRT application, EB-RGD was labelled with ^{177}Lu, which emits β rays. Through this investigation, we aimed to investigate whether PDXs could reproduce the same characteristics of the corresponding parental NSCLC and explore whether the ^{177}Lu-EB-RGD could be used as a novel therapeutic approach in patients with advanced NSCLC.

Materials and methods

PDX establishment

Patient written informed consent was obtained, and the research protocol was approved by the Clinical Research Ethics Committee of the First Affiliated Hospital of Xiamen University (ID KYZ2017–001). All animal care and experimental procedures were reviewed and approved by the Animal Care and Use Committee of Xiamen University Laboratory Animal Center (ID XMULAC20170063). The tumour specimens were obtained from patients who underwent presurgical ^{18}F-FDG PET/CT. After surgical resection, NSCLC specimens were immediately placed in DMEM (Cat. #C11995599BT, Gibco, USA) supplemented with 2% antibiotics (penicillin, streptomycin) and transferred into the ice box.

Immunodeficient BALB/c nude mice were bred under sterile conditions in Xiamen University Laboratory Animal Center from founders originally obtained from Charles River Co., Ltd (Beijing, China). To establish PDXs, a fresh tumour specimen was processed into approximately 30 mm^3 for implantation subcutaneously (s.c.) at the level of trans-scapular brown fat of 4–6 weeks BALB/c Nude female mice within an average of 2 hours following the patient's surgery. Tumour growth was monitored at least twice weekly using callipers until it reached a maximal volume of 1500 mm^3, after which the mouse was euthanised by cervical dislocation, and the tumour was removed. The tumour was minced with scissors and tumour fragments were implanted in BALB/c Nude mice; the remaining fragments were used for histopathological analyses. For investigational purposes, PDXs were expanded in a higher number of mice to obtain statistically relevant results.

Radiochemistry

Cyclic-RGD peptide was purchased from C.S. Bio for research purpose. EB-RGD was synthesised as previously described[13]. Details of synthetic procedures and characterisation of chemical components are described in the supplemental materials (Supplemental Fig. 1). High-purity radionuclide ^{177}Lu was purchased from ITG (Germany) in a solution of ^{177}LuCl$_3$. For radiolabelling, 1.85 GBq of ^{177}LuCl$_3$ was diluted using 4 mL of 0.05 M HCl. EB-RGD (100 μg), or RGD (100 μg) was dissolved in 1 mL of 0.25 M NH$_4$OAc (pH = 5.6), and subsequently added to the ^{177}LuCl$_3$. The mixture was heated at 90 °C for 30 mins; a C$_{18}$ column was used for purifying and a 0.22-μm filtration membrane was used to ensure sterility. Next, 1 mL ethanol of 60% volume fraction was injected into the product container through a C$_{18}$ column and aseptic filtration membrane; further, 5 mL normal saline was added. The ethanol concentration in the solution was about 10% when the tail vein was injected. Analytical thin-layer chromatography (Bioscan, USA) was used for radiochemical purity control. Moreover, we evaluated the ^{177}Lu-EB-RGD stability both *in vitro* and *in vivo*; the methodology for the stability assays can be found in the supplemental material.

SPECT imaging and biodistribution study in NSCLC-PDX models

Single-photon emission computer tomography (SPECT) was performed with the Mediso (Hungary) multi-pinhole camera; 18.5 MBq of ^{177}Lu-EB-RGD or ^{177}Lu-RGD were intravenously injected into NSCLC-PDXs (n = 4). Whole-body SPECT imaging was performed as described previously[12]. The acquisition times were at 4, 24, 48, 72, and 96 hours post injection (p.i.). Regions of interest (ROIs) of the tumour, liver, heart, and muscle were counted on the SPECT images to quantify the radioactive signals, which were recorded as blood-to-muscle (B/M), tumour-to-muscle (T/M), and liver-to-muscle (L/M) ratios.

In the biodistribution study, groups of NSCLC-PDXs were injected with the same batch (same specific activities) of 0.5 MBq ^{177}Lu-EB-RGD and were sacrificed at different times (4, 24, 48, and 72 hours p.i.; n = 3 for each time point, 12 mice for each group). The main organs and tumour were weighed and analysed. The ^{177}Lu-RGD group biodistribution was performed for contrasting as well. Groups of NSCLC-PDXs were sacrificed at 24 hours p.i. (n = 3 for each group). The γ-counter (WIZARD 2480; USA) was used for assaying radioactivity.

The *in vivo* distribution pattern of EB-RGD and RGD was further evaluated via dynamic PET scan (using ^{68}Ga-EB-RGD and ^{68}Ga-RGD as the PET tracer) in healthy BALB/C mice. The half-life of EB-RGD and RGD were calculated by drug and statistics software (DAS version 2.0). The methodology for the dynamic PET scan can be found in the supplemental material.

In vivo therapy regimen

NSCLC-PDXs were used for *in vivo* therapy study when the tumour volume reached approximately 100 mm^3. NSCLC-PDXs were divided into four groups (9 – 10 mice/group): Group A, 100ul saline; Group B, 29.6 MBq of ^{177}Lu-RGD; Group C, 18.5 MBq of ^{177}Lu-EB-RGD; Group D, 29.6 MBq of ^{177}Lu-EB-RGD (all drugs was injected through intravenous (i.v.).

Tumour volume and body weight were recorded each 2 days. The formula: (length × width × width)/2 was used to calculated tumour volume. Three days after the beginning of treatment, groups A–D (n = 3) from NSCLC-PDXs underwent ^{18}F-FDG PET (Inveon, Siemens) imaging. The ^{18}F-FDG PET imaging protocol was performed as previously described[14].

The endpoint criteria for mice were as follows: tumour volume >1,500 mm^3, weight loss >20%, or active tumour ulceration.

Histopathological staining

Animal tumour specimens from each group were sectioned at day 14 after treatment. CD31 immunohistochemistry (IHC) was used to picture the endothelial cells. The primary antibodies of this experiment were anti-mouse CD31 mAb (ab9498; Abcam, Cambridge, United Kingdom), Ki-67-specific mAb (ab15580; Abcam, Cambridge, United Kingdom), human integrin $\alpha_v\beta_3$ (ab7166; Abcam, Cambridge, United Kingdom), and murine integrin $\alpha_v\beta_3$ (CD61, Novus Biologicals, SJ19–09). Using these markers, routine IHC staining was performed according to our previous protocol[13]. The expression of integrin $\alpha_v\beta_3$ was further detected by Western blot analysis; the protocol can be found in the supplemental material. A commercially available kit (Roche Applied Science) was for immunofluorescent TdT-mediated dUTP Nick-End Labelling (TUNEL) analysis. Haematoxylin and eosin (H&E) staining was procured by Univ-Bio Inc.

Statistics

All quantitative data are expressed as mean ± SD. All statistical analyses were conducted by using SPSS 22.0 statistical analysis software (IBM, Armonk, NY, USA). One-way analysis of variance and Student's *t* test were used to compare means. A *P* value of < 0.05 was considered statistically significant.

Results

Radiolabelled compounds preparation

Two radioligands with high affinity for integrin $\alpha_v\beta_3$ were prepared in this study: ^{177}Lu-EB-RGD and ^{177}Lu-RGD, both of which had >95% radiochemical purity after purification.

^{177}Lu-RGD and ^{177}Lu-EB-RGD were radiolabelled at an average specific activity of 18.6 ± 4.7 and 55.85 ± 14.0 GBq/μmol, respectively.

Stability of ^{177}Lu-EB-RGD

^{177}Lu-EB-RGD was stable in mouse serum for up to 24 h with no significant de-metalation observed. *In vivo*, over 90% of the radioactivity was bound to the blood proteins and not extractable. The extracted radioactivity showed ^{177}Lu-EB-RGD with only a small amount of a more polar component appearing at 4 h after i.v. injection.

NSCLC-PDXs establishment and validation

Fragments of primary tumour tissues were collected from eight patients who underwent surgical resection, and the diagnosis of NSCLC was confirmed by histopathology. The small fragments of primary tumour tissues were subsequently implanted into eight groups of immunodeficient BALB/c Nude mice for propagation. Finally, three different groups of NSCLC-PDXs were successfully established, all of which were derived from adenocarcinomas. The three groups had different clinical stages (1 stage IB, 1 stage IIA, and 1 stage IIIA), different degrees of lymph node involvement (1 N0, 1 N1, and 1 N3) and different degrees of integrin $\alpha_v\beta_3$ expression levels (1 intense, 1 moderate, and 1 low expression). No driver mutations were observed in any of the three groups. The latency times (time interval from implantation to presence of palpable tumour) (range, 23.3–65.6 days post implantation) and tumour growth rate (Supplemental Fig. 2) varied in the three groups. The phenotype of each NSCLC patient is summarised in Supplemental Table 1. All these parameters were consistent between the NSCLC-PDXs and their corresponding primary NSCLC (Supplemental Table 2), confirming the unique nature of individual PDXs. The two NSCLC-PDXs groups with intense and low integrin $\alpha_v\beta_3$ expression (denoted as $PDX_{\alpha v\beta3+}$ and $PDX_{\alpha v\beta3-}$) were chosen as the experimental models to evaluate the *in vivo* biological behaviour of ^{177}Lu-EB-RGD. It is worth noting that integrin $\alpha_v\beta_3$ is expressed on both tumour cells and neovasculature. Although $PDX_{\alpha v\beta3-}$ tumours have low expression of integrin $\alpha_v\beta_3$ on the tumour cells, they show high levels of murine vascular integrin expression (CD61, murine integrin $\alpha_v\beta_3$). The PET imaging and histopathology information from the two PDX groups and their parental tumours are presented in Figure 1.

SPECT imaging and biodistributions of ^{177}Lu-EB-RGD in NSCLC-PDXs

Whole-body SPECT imaging studies were performed for exploring the *in vivo* behaviour of ^{177}Lu-EB-RGD. Representative whole-body Maximum Intensity Projections (MIP) of $PDX_{\alpha v\beta3+}$ and $PDX_{\alpha v\beta3-}$ are presented in Figure 2.

SPECT imaging of ^{177}Lu-EB-RGD in $PDX_{\alpha v\beta3+}$ is shown in Figure 2A. High tumour-to-background ratio was observed at 4 h p.i. (T/M: 7.34 ± 0.67), and elevated at 24 and 48h p.i., with tumour uptake peaking at 72 h p.i. (T/M: 15.99 ± 5.42) and reducing slightly from 96 to 120 h p.i. Blood ^{177}Lu-EB-RGD uptake was comparatively high at 1 h p.i. (B/M: 4.31 ± 1.22), and decreased from 24 to 120 h p.i. gradually. The kidneys also showed a ^{177}Lu signal, which gradually decreased from 24 to 120 h p.i. As shown in Figure 2B, ^{177}Lu-EB-RGD uptake in $PDX_{\alpha v\beta3-}$ was significantly lower than that in $PDX_{\alpha v\beta3+}$ at all time points. The T/M ratio in $PDX_{\alpha v\beta3-}$ from 4 to 96 h p.i were 4.18 ± 0.74, 5.17 ± 4.11, 6.97 ± 1.12,

6.62 ± 1.64 and 7.34 ± 0.67, respectively. ^{177}Lu-RGD SPECT imaging in both $PDX_{\alpha v \beta 3+}$ and $PDX_{\alpha v \beta 3-}$ was also performed for comparison (Figure 2A, B). ^{177}Lu-RGD was shown to be cleared from the blood rapidly and showed a significantly low accumulation in both PDXs at 24 h p.i.

The biodistributions of ^{177}Lu-EB-RGD in the two PDX groups were obtained at different time points p.i. (Figure 3). The biodistributions results were generally in line with previous SPECT imaging studies. In the case of $PDX_{\alpha v \beta 3+}$ (Figure 3A), ^{177}Lu-EB-RGD accumulated mainly in the blood (12.99 ± 1.54 %ID/g) at 4 h p.i. Moreover, ^{177}Lu-EB-RGD uptake was also observed in the kidney (9.81 ± 1.83 %ID/g), liver (7.56 ± 4.89 %ID/g), and spleen (7.87 ± 1.95 %ID/g). Tumour uptake at this time was 10.75 ± 1.17 %ID/g. ^{177}Lu-EB-RGD in the blood, kidneys, liver, and spleen had decreased to 4.41 ± 0.45, 8.99 ± 0.99, 6.06 ± 0.65, and 5.61 ± 2.67 %ID/g at 24 h p.i., respectively, while the tumour uptake had increased to 13.38 ± 1.04 %ID/g. ^{177}Lu-EB-RGD uptake in tumour had reached its peak (14.87 ± 6.71 %ID/g) at 48 h p.i., whereas the uptake in blood (1.71 ± 0.35 %ID/g), kidneys (7.78 ± 1.58 %ID/g), liver (5.60 ± 0.75 %ID/g), and spleen (5.23 ± 1.04 %ID/g) had continued to decrease. At 72 h p.i., ^{177}Lu-EB-RGD further clearance from all organs was observed. A similar *in vivo* distribution pattern was observed in $PDX_{\alpha v \beta 3-}$ (Figure 3B), except for the significantly reduced tumour uptake at all time points tested (^{177}Lu-EB-RGD uptakes in $PDX_{\alpha v \beta 3-}$ from 4–72 h p.i. were 4.89 ± 1.33, 6.25 ± 0.56, 6.47 ± 1.50, and 5.55 ± 2.05 %ID/g, respectively).

The ^{177}Lu-RGD biodistribution was also investigated for comparison (Figure 3C–D). In accordance with the SPECT findings, ^{177}Lu-RGD demonstrated a much shorter blood half-life than ^{177}Lu-EB-RGD in both PDX groups. The blood uptake of ^{177}Lu-RGD was almost 15 times lower than ^{177}Lu-EB-RGD at 24 h p.i. Therefore, ^{177}Lu-EB-RGD demonstrated a significantly higher tumour uptake in both $PDX_{\alpha v \beta 3+}$ (13.38 ± 1.04 *vs.* 2.59 ± 1.60 %ID/g) and $PDX_{\alpha v \beta 3-}$; (6.26 ± 0.56 *vs.* 1.56 ± 0.35 %ID/g). The promising high tumour uptake of ^{177}Lu-EB-RGD and prolonged tumour retention time resulted in high exposure to the radioactive isotope. The area under the curve calculated from the radioactivity accumulation in tumours over time is shown in Supplemental Fig. 3.

Furthermore, the pharmacokinetic parameters of EB-RGD and RGD were calculated by dynamic PET scan (Supplemental Fig. 4), which demonstrated that intravenously administered RGD was cleared from the circulation rapidly with a $t_{1/2}$ of 33.4 ± 0.9 min. The $t_{1/2}$ of EB-RGD was 167.8 ± 19.7 min, a 5-fold longer half-life than that of RGD.

^{177}Lu-EB-RGD demonstrates significant antitumoral radiotherapy efficacy in NSCLC-PDXs

To investigate whether ^{177}Lu-EB-RGD TRT would be efficacious in NSCLC-PDXs, the antitumoral radiotherapy efficacy of ^{177}Lu-EB-RGD was first evaluated in the $PDX_{\alpha v \beta 3+}$ subjects, which were divided into four groups (A–D) and monitored for 50 days post treatment. The Figure 4A showed therapy protocols along with the mice relative tumour volumes and body weigh.

Transient weight loss was observed in this PDX, and the mice regained their starting weight by the end of the study. (Figure 4B). Group A (saline) and group B (29.6 MBq of ^{177}Lu-RGD) showed rapid tumour growth. All PDXs in groups A and B had to be euthanised by

day 36 because of excessive tumour volume (Figure 4C, pink and purple lines). To evaluate the appropriate therapy dose of ^{177}Lu TRT, ^{177}Lu-EB-RGD was delivered in a radioactive dose of either 18.5 MBq (Group C) or 29.6 MBq (Group D). In groups C and D, significant inhibition of tumour growth could be seen (Figure 4C). ^{77}Lu-EB-RGD and saline-treated groups showed significant difference in tumour volume starting from day 4 (P = 0.007), while ^{177}Lu-EB-RGD and ^{177}Lu-RGD group demonstrated significant difference starting from day 6 (P = 0.001). These differences increased over time; most tumours in the ^{177}Lu-EB-RGD therapy groups began to shrink from day 6 and completely disappeared at day 24. Although Group D showed a faster tumour inhibition rate as compared to Group C, all of the PDXs (9/9, 100%) in both groups finally showed a complete response (CR), with all of these CR maintaining for the duration of the 50 days study. Kaplan-Meier curves based on the protocol endpoints showed significant differences (P < 0.001) between groups A–B and groups C–D, but no significant difference was observed between groups C and D (Figure 4D). The survival rate in the two ^{177}Lu-EB-RGD-treated groups were both maintained at 100% up to day 50 after the initial treatment. Therefore, a therapy dose of 18.5 MBq ^{177}Lu-EB-RGD may be strong enough for tumour elimination in the PDXs with intense integrin $\alpha_v\beta_3$ expression.

During treatment, early therapeutic response was evaluated by ^{18}F-FDG PET at day 3 after treatment. The representative ^{18}F-FDG PET images of four therapy groups are presented in Figure 4E. Compared to the saline control and ^{177}Lu-RGD-treated groups, significantly decreased ^{18}F-FDG uptake was observed in the ^{177}Lu-EB-RGD-treated groups (Figure 4F), indicating reduced tumour metabolism following ^{177}Lu TRT.

We also tested the therapeutic efficacy of ^{177}Lu-EB-RGD in the NSCLC-PDXs with low expression (PDX$_{\alpha v\beta3-}$), using the same therapy protocol among four groups (Figure 5A). Once again, transient weight loss due to ^{177}Lu TRT was observed in these PDX$_{\alpha v\beta3-}$, although the extent of wight loss was lower than that of PDX$_{\alpha v\beta3+}$. (Figure 5B). The tumour volumes in the two ^{177}Lu-EB-RGD-treated groups were similar to those in the control and ^{177}Lu-RGD-treated groups up to day 8 after treatment, and then a minor tumour volume reduction was observed in both of the ^{177}Lu-EB-RGD-treated groups, which lasted for several days. However, the tumour volumes in the ^{177}Lu-EB-RGD-treated groups increased once more from day 14 onward but grew at a slower rate than in the control and ^{177}Lu-RGD-treated groups. In other words, ^{177}Lu-EB-RGD-targeted radionuclide therapy led to a delay in tumour growth in the PDX$_{\alpha v\beta3-}$, rather than tumour shrinkage, as shown in PDX$_{\alpha v\beta3+}$ (Figure 5C).

Tumour biology evaluated by immunohistochemistry

As shown in Figure 6, Groups C and D (18.5 and 29.6 MBq ^{177}Lu-EB-RGD) displayed a much lower extent of tumour vasculature than did Groups A and B (saline and 29.6 MBq ^{177}Lu-RGD). Groups A and B demonstrated a relatively higher percentage of cells that stained positively for Ki-67, while groups C and D demonstrated reduced cell proliferation. Regarding TUNEL staining, both ^{177}Lu-EB-RGD groups showed considerably more cell apoptosis compared to groups A and B. H&E staining showed extensive necrotic areas for the ^{177}Lu-EB-RGD-treated groups, whereas tumours from the saline control and ^{177}Lu-

RGD-treated groups only showed necrotic areas in the middle of the tumour. To further test the possible toxicity effects of ^{177}Lu-EB-RGD, pathological examination of H&E staining of selected non-cancerous organs was performed, which revealed no obvious differences between the ^{177}Lu-treated and control groups (Supplemental Fig. 5).

The IHC results in the $PDX_{\alpha v \beta 3-}$ groups were similar to those in the $PDX_{\alpha v \beta 3+}$ groups, except that fewer necrotic areas of $PDX_{\alpha v \beta 3-}$ were observed in ^{177}Lu-EB-RGD-treated groups as compared to those in $PDX_{\alpha v \beta 3+}$ (Supplemental Fig. 6).

DISCUSSION

Current chemotherapy regimens have unsatisfactory results in most advanced NSCLC. Targeted therapies and immunotherapies represent two of the most researched types of therapy under current investigation for the treatment of NSCLC[4]. However, over 80% of patients with advanced NSCLC do not have oncogenic driver biomarker status and resistance is inevitable[4]. Immunotherapy, especially ICB therapy, provides the hope that long-term survival is achievable in a subset of patients, but the ICB therapy could only benefit to a small population of patients[15]. It is therefore imperative to develop novel therapeutic strategies and to optimize selection of patients, identifying early those who could benefit from available treatments.

Mouse tumour models are the most valuable tool for preclinical evaluation of novel therapeutic strategies in cancer[16]. However, some drugs that show therapeutic efficacy against human tumour xenografts have often failed to show activity in human clinical trials[17,18], resulting in an imperfect correlation between preclinical and clinical results in terms of therapeutic efficacy. Recently, some studies have demonstrated that PDXs have great potential in drug development studies since they reliably reproduce the patient's parental tumour for both IHC markers and genetic alterations as well as for evaluating the response to the corresponding therapeutic regimens. Moreover, PDXs accurately reproduce the heterogeneity of human cancers and maintain at least some aspects of the human microenvironment; therefore, they represent a promising preclinical model for studies of tumour heterogeneity and tumour-microenvironment studies[19,20]. As such, we investigated the establishment of PDXs from NSCLC as a source of therapeutically relevant information. As expected, our results demonstrated that PDXs derived from NSCLC can maintain the same immunohistochemical and genetic characterization of the human primary tumour, confirming the robustness of this model to test the efficacy of new treatments for NSCLC. Moreover, in our experience, the growth features of PDX (such as latency time and tumour growth rate) reach stability after 3–4 passages in mice; it is therefore advisable to carry out drug efficacy evaluation with PDXs that have reached a certain stability in their growth characteristics.

We have further confirmed the robustness of the PDXs by using PET imaging, which showed concordant uptake of ^{18}F-FDG between primary NSCLC and corresponding PDXs. Interestingly, lower ^{18}F-FDG uptake was observed in PDXs with lower integrin $\alpha_v \beta_3$ expression. This may be partially explained by the finding that both integrin $\alpha_v \beta_3$ expression and ^{18}F-FDG uptake are correlated with tumour aggressiveness and prognosis in NSCLC[21].

However, it cannot be concluded that ^{18}F-FDG provides information similar to that of an RGD-based tracer, because both tracers have completely different pharmacodynamic properties. In a previous study[22], Beer et al. compared the ^{18}F-RGD uptake and ^{18}F-FDG uptake on PET in primary and metastatic tumour lesions in cancer patients, and found no substantial correlation between ^{18}F-RGD and ^{18}F-FDG uptake, suggesting that $\alpha_v\beta_3$ expression and glucose metabolism are not closely linked in malignant lesions.

Targeted radionuclide therapy (TRT) is the use of radioisotopes to deliver ionization energy to tumour cells[8]. TRT is particularly useful in cases of metastatic disease where conventional treatments are no longer effective[7,23]. According to previous clinicals trials in NETs and CRPC, ^{177}Lu TRT results in high responses, a low toxicity profile, and improves overall survival[23,24]. As such, TRT may also provide a novel strategy for the treatment of advanced NSCLC. Although several preclinical studies have demonstrated the significant anti-tumour efficacy of TRT in lung cancer mouse models[4], no clinical trial until now has provided a clue as to whether this approach holds promise or not. In our present study, we chose RGD peptide as the TRT vector for targeting the integrin $\alpha_v\beta_3$ receptor, which has been validated to be overexpressed in NSCLC and to have a crucial role in tumour angiogenesis[11]. More importantly, the pharmacokinetics of the targeting vector RGD were further improved by conjugation of RGD with an albumin binding moiety, the truncated EB. The reversible binding of EB to albumin has been well documented, with a stoichiometry of 8–14 dye molecules per molecule of albumin[25]. In our previous study[13], we demonstrated that albumin can serve as a pool and allow the slow release of EB-RGD from albumin. The slow release of drug over time would allow continual uptake at the biological target (integrin $\alpha_v\beta_3$ on tumour cells and vasculature). Furthermore, the internalization assays in our previous study have found that most of the EB-RGD was internalised into tumour cells (due to $\alpha_v\beta_3$ receptor-mediated internalization), while the albumin was not internalised in the presence of EB-RGD.

The improved pharmacokinetics of EB-RGD, demonstrated by both a longer-half life and higher retention in the blood pool, resulted in significantly higher accumulation of ^{177}Lu-EB-RGD and enhanced tumour to background ratios as shown in SPECT imaging and biodistribution studies. The anti-tumour efficacy of ^{177}Lu-EB-RGD in NSCLC-PDXs is also quite impressive: a therapeutic dose of 18.5 MBq ^{177}Lu-EB-RGD was enough to completely eradicate the NSCLC-PDXs with high integrin $\alpha_v\beta_3$ expression, with no sign of tumour recurrence during the observation period. Considering integrin $\alpha_v\beta_3$ is expressed on both tumour cells and neovasculature, ^{177}Lu-EB-RGD was able to target both tumour cells and tumour vasculature, as confirmed by the reduced expression of CD31 (a vascularization marker) and Ki-67 (a proliferation marker) after treatment.

Such TRT treatment was also efficacious even in the NSCLC- PDXs with low integrin $\alpha_v\beta_3$ expression; a therapeutic dose of 29.6 MBq ^{177}Lu-EB-RGD led to a significant delay in tumour growth as compared to control or ^{177}Lu-RGD monomer group. The modest therapeutic effect observed in this PDX may be due to the following reason: the tumour uptake of ^{177}Lu-EB-RGD can be divided into three portions, the expression of integrin $\alpha_v\beta_3$ on tumour cells and on neovasculature, as well as the reinforced vascular permeability and retention (EPR) effect. Although PDX$_{\alpha v\beta_3-}$ models have low expression of integrin $\alpha_v\beta_3$

within the tumour cells, they exhibit high levels of murine vascular integrin $\alpha_v\beta_3$ expression (as confirmed by CD61 IHC staining). From the biodistribution study, ^{177}Lu-EB-RGD uptake in $PDX_{\alpha v\beta 3-}$ was about half that of $PDX_{\alpha v\beta 3+}$ tumour uptake (13.38 %ID/g vs. 6.26 %ID/g), which means 50% of tumour uptake may have been due to uptake by the neovasculature and EPR effect. The remaining 50% of ^{177}Lu-EB-RGD uptake in tumour could explain the observed therapeutic effect on PDX tumours with low integrin expression. Furthermore, we could also observe the reduced expression of CD31 in the $PDX_{\alpha v\beta 3-}$ tumours, suggesting that the modest therapeutic effect is partly due to the damage to the tumour vasculature.

In future clinical translation, ^{68}Ga/^{177}Lu-RGD theranostics could enable a highly personalised approach using ^{68}Ga-RGD PET/CT to non-invasively image and quantify integrin $\alpha_v\beta_3$ expression, and thereby select the patients most likely to benefit from treatment. ^{68}Ga-RGD PET/CT can also be used to evaluate the response to therapy after ^{177}Lu-EB-RGD treatment; further therapy cycles can be cancelled if there is no or low uptake on post-treatment PET imaging (indicative of a complete or partial response). The principles and expertise required in RGD-based NSCLC theranostics broadly parallel those using ^{68}Ga/^{177}Lu-labelled DOTATATE for metastatic NETs[26,27] or PSMA for metastatic CRPC[24,28]. However, based on previous trials using peptide receptor radionuclide therapy (PRRT) or peptide radioligand therapy (PRLT), three to four cycles of ^{177}Lu-DOTATATE/ ^{177}Lu-PSMA are usually required for an entire treatment paradigm, and each cycle requires a dose of at least 1.85–7.4 GBq of ^{177}Lu, resulting in a total dosage of 7.4–29.6 GBq ^{177}Lu[26,29–31]. Such a huge radiation dosage may result in treatment-related toxic effects on normal organs, such as salivary gland dysfunction, loss of kidney function, and haematological toxicity. However, according to our experience using ^{177}Lu-EB-TATE or ^{177}Lu-EB-PSMA[32,33], a single dose of 1.85–3.70 GBq ^{177}Lu provides comparable therapeutic efficacy due to the enhanced tumour accumulation and prolonged retention of such EB derivatives. Unexpectedly, a single imaging dose (0.67–0.8 GBq) of ^{177}Lu-EB-TATE /^{177}Lu-EB-PSMA provides some therapeutic efficacy in some patients with NETs or CRPCs. The approximately 6-fold lower dosage of ^{177}Lu and reduced dosing frequency would greatly decrease the potential side effects and increase patient compliance.

Besides the pharmacokinetics of radiotherapeutic agents, barriers to the success of TRT include the heterogeneous expression of molecular markers on cancer cells and poor vasculature of the tumour, which would prevent delivery of the agents[34]. In addition, the biological response to TRT of individual cells within a tumour may vary depending on cell-specific radiosensitivity to the radiotherapeutic agent[35]. Other variables that are important in TRT include the biological effectiveness of the emitted particles, dose rate and the induction of bystander responses[36]. These properties of TRT may be exploitable in rationally designed combination protocols that aim to complement the strengths of TRT with other therapeutics and take into consideration optimal timing and sequencing. In our latest study, the combination of TRT (^{177}Lu-EB-RGD) and immune checkpoint inhibitors (anti-PD-L1 antibodies) in MC38 colon cancer xenografts enhanced mice survival significantly as compared with that of TRT or immunotherapy alone[12]. This combination may represent a promising approach for metastatic tumours in which TRT can be used. Therefore, a concentrated effort is needed to shift research from preclinical studies to randomised trials of

combination treatments if the potential of TRT is to be fully exploited. The integration of TRT into first-line therapy, rather than as a treatment for end-stage disease (which has been the norm to date) is predicted to be beneficial in the future.

In conclusion, we have designed a theranostic agent, based on an RGD peptide, that targets integrin $\alpha_v\beta_3$-expressing NSCLC and demonstrates improved pharmacokinetics. Using the β-emitting radionuclide ^{177}Lu, we obtain improved contrast for SPECT imaging and effective TRT for NSCLC-PDXs. Furthermore, our PDX models maintain the same immunohistochemical and genetic characteristics of the human primary tumour. These preclinical data suggest that ^{177}Lu- EB-RGD may be an effective treatment option for NSCLC that should be further evaluated in human trials.

Supplementary Material

Refer to Web version on PubMed Central for supplementary material.

Acknowledgments

References

1. Bray F, Ferlay J, Soerjomataram I, et al. Global cancer statistics 2018: GLOBOCAN estimates of incidence and mortality worldwide for 36 cancers in 185 countries. CA Cancer J Clin. 11 2018;68:394–424. [PubMed: 30207593]

2. Ettinger DS, Akerley W, Bepler G, et al. Non-small cell lung cancer. J Natl Compr Canc Netw. 7 2010;8:740–801. [PubMed: 20679538]

3. Schiller JH, Harrington D, Belani CP, et al. Comparison of four chemotherapy regimens for advanced non-small-cell lung cancer. N Engl J Med. 1 10 2002;346:92–98. [PubMed: 11784875]

4. Naylor EC, Desani JK, Chung PK. Targeted Therapy and Immunotherapy for Lung Cancer. Surg Oncol Clin N Am. 7 2016;25:601–609. [PubMed: 27261918]

5. Cortot AB, Janne PA. Molecular mechanisms of resistance in epidermal growth factor receptor-mutant lung adenocarcinomas. Eur Respir Rev. 9 2014;23:356–366. [PubMed: 25176972]

6. Mok TSK, Wu YL, Kudaba I, et al. Pembrolizumab versus chemotherapy for previously untreated, PD-L1-expressing, locally advanced or metastatic non-small-cell lung cancer (KEYNOTE-042): a randomised, open-label, controlled, phase 3 trial. Lancet. 5 4 2019;393:1819–1830. [PubMed: 30955977]

7. Iikuni S, Ono M, Watanabe H, et al. Cancer radiotheranostics targeting carbonic anhydrase-IX with (111)In- and (90)Y-labeled ureidosulfonamide scaffold for SPECT imaging and radionuclide-based therapy. Theranostics. 2018;8:2992–3006. [PubMed: 29896298]

8. Pouget JP, Navarro-Teulon I, Bardies M, et al. Clinical radioimmunotherapy--the role of radiobiology. Nat Rev Clin Oncol. 11 8 2011;8:720–734. [PubMed: 22064461]

9. FDA Approves Lutathera for GEP NET Therapy. J Nucl Med. 4 2018;59:9N.

10. Chen H, Niu G, Wu H, et al. Clinical Application of Radiolabeled RGD Peptides for PET Imaging of Integrin alphavbeta3. Theranostics. 2016;6:78–92. [PubMed: 26722375]

11. Zheng K, Liang N, Zhang J, et al. 68Ga-NOTA-PRGD2 PET/CT for Integrin Imaging in Patients with Lung Cancer. J Nucl Med. 12 2015;56:1823–1827. [PubMed: 26429958]

12. Chen H, Zhao L, Fu K, et al. Integrin alphavbeta3-targeted radionuclide therapy combined with immune checkpoint blockade immunotherapy synergistically enhances anti-tumor efficacy. Theranostics. 2019;9:7948–7960. [PubMed: 31695808]

13. Chen H, Jacobson O, Niu G, et al. Novel "Add-On" Molecule Based on Evans Blue Confers Superior Pharmacokinetics and Transforms Drugs to Theranostic Agents. J Nucl Med. 4 2017;58:590–597. [PubMed: 27879373]

14. Wu H, Chen H, Pan D, et al. Imaging integrin alphavbeta 3 and NRP-1 positive gliomas with a novel fluorine-18 labeled RGD-ATWLPPR heterodimeric peptide probe. Mol Imaging Biol. 12 2014;16:781–792. [PubMed: 25001194]

15. Osmani L, Askin F, Gabrielson E, et al. Current WHO guidelines and the critical role of immunohistochemical markers in the subclassification of non-small cell lung carcinoma (NSCLC): Moving from targeted therapy to immunotherapy. Semin Cancer Biol. 10 2018;52:103–109. [PubMed: 29183778]

16. Chow LQ, Eckhardt SG. Sunitinib: from rational design to clinical efficacy. J Clin Oncol. 3 1 2007;25:884–896. [PubMed: 17327610]

17. Burchill SA. What do, can and should we learn from models to evaluate potential anticancer agents? Future Oncol. 4 2006;2:201–211. [PubMed: 16563089]

18. Voskoglou-Nomikos T, Pater JL, Seymour L. Clinical predictive value of the in vitro cell line, human xenograft, and mouse allograft preclinical cancer models. Clin Cancer Res. 9 15 2003;9:4227–4239. [PubMed: 14519650]

19. Blomme A, Van Simaeys G, Doumont G, et al. Murine stroma adopts a human-like metabolic phenotype in the PDX model of colorectal cancer and liver metastases. Oncogene. 3 2018;37:1237–1250. [PubMed: 29242606]

20. DeRose YS, Wang G, Lin YC, et al. Tumor grafts derived from women with breast cancer authentically reflect tumor pathology, growth, metastasis and disease outcomes. Nat Med. 10 23 2011;17:1514–1520. [PubMed: 22019887]

21. Higashi K, Ito K, Hiramatsu Y, et al. 18F-FDG uptake by primary tumor as a predictor of intratumoral lymphatic vessel invasion and lymph node involvement in non-small cell lung cancer: analysis of a multicenter study. J Nucl Med. 2 2005;46:267–273. [PubMed: 15695786]

22. Beer AJ, Lorenzen S, Metz S, et al. Comparison of integrin alphaVbeta3 expression and glucose metabolism in primary and metastatic lesions in cancer patients: a PET study using 18F-galacto-RGD and 18F-FDG. J Nucl Med. 1 2008;49:22–29. [PubMed: 18077538]

23. Kessel K, Seifert R, Schafers M, et al. Second line chemotherapy and visceral metastases are associated with poor survival in patients with mCRPC receiving (177)Lu-PSMA-617. Theranostics. 2019;9:4841–4848. [PubMed: 31410185]

24. Hofman MS, Violet J, Hicks RJ, et al. [(177)Lu]-PSMA-617 radionuclide treatment in patients with metastatic castration-resistant prostate cancer (LuPSMA trial): a single-centre, single-arm, phase 2 study. Lancet Oncol. 6 2018;19:825–833. [PubMed: 29752180]

25. Lindner V, Heinle H. Binding properties of circulating Evans blue in rabbits as determined by disc electrophoresis. Atherosclerosis. 6 1982;43:417–422. [PubMed: 7115470]

26. Wolf KI, Jha A, van Berkel A, et al. Eruption of Metastatic Paraganglioma After Successful Therapy with (177)Lu/(90)Y-DOTATOC and (177)Lu-DOTATATE. Nucl Med Mol Imaging. 6 2019;53:223–230. [PubMed: 31231443]

27. Waldmann CM, Stuparu AD, van Dam RM, et al. The Search for an Alternative to [(68)Ga]Ga-DOTA-TATE in Neuroendocrine Tumor Theranostics: Current State of (18)F-labeled Somatostatin Analog Development. Theranostics. 2019;9:1336–1347. [PubMed: 30867834]

28. Lindstrom E, Velikyan I, Regula N, et al. Regularized reconstruction of digital time-of-flight (68)Ga-PSMA-11 PET/CT for the detection of recurrent disease in prostate cancer patients. Theranostics. 2019;9:3476–3484. [PubMed: 31281491]

29. Roll W, Bode A, Weckesser M, et al. Excellent Response to 177Lu-PSMA-617 Radioligand Therapy in a Patient With Advanced Metastatic Castration Resistant Prostate Cancer Evaluated by 68Ga-PSMA PET/CT. Clin Nucl Med. 2 2017;42:152–153. [PubMed: 27922871]

Author Manuscript Author Manuscript Author Manuscript Author Manuscript

30. Heinzel A, Boghos D, Mottaghy FM, et al. (68)Ga-PSMA PET/CT for monitoring response to (177)Lu-PSMA-617 radioligand therapy in patients with metastatic castration-resistant prostate cancer. Eur J Nucl Med Mol Imaging. 5 2019;46:1054–1062. [PubMed: 30697649]

31. Grubmuller B, Senn D, Kramer G, et al. Response assessment using (68)Ga-PSMA ligand PET in patients undergoing (177)Lu-PSMA radioligand therapy for metastatic castration-resistant prostate cancer. Eur J Nucl Med Mol Imaging. 5 2019;46:1063–1072. [PubMed: 30569186]

32. Wang H, Cheng Y, Zhang J, et al. Response to Single Low-dose (177)Lu-DOTA-EB-TATE Treatment in Patients with Advanced Neuroendocrine Neoplasm: A Prospective Pilot Study. Theranostics. 2018;8:3308–3316. [PubMed: 29930731]

33. Zang J, Fan X, Wang H, et al. First-in-human study of (177)Lu-EB-PSMA-617 in patients with metastatic castration-resistant prostate cancer. Eur J Nucl Med Mol Imaging. 1 2019;46:148–158. [PubMed: 30090965]

34. Gill MR, Falzone N, Du Y, et al. Targeted radionuclide therapy in combined-modality regimens. Lancet Oncol. 7 2017;18:e414–e423. [PubMed: 28677577]

35. Rajon D, Bolch WE, Howell RW. Survival of tumor and normal cells upon targeting with electron-emitting radionuclides. Med Phys. 1 2013;40:014101. [PubMed: 23298125]

36. Prise KM, Folkard M, Michael BD. Bystander responses induced by low LET radiation. Oncogene. 10 13 2003;22:7043–7049. [PubMed: 14557809]
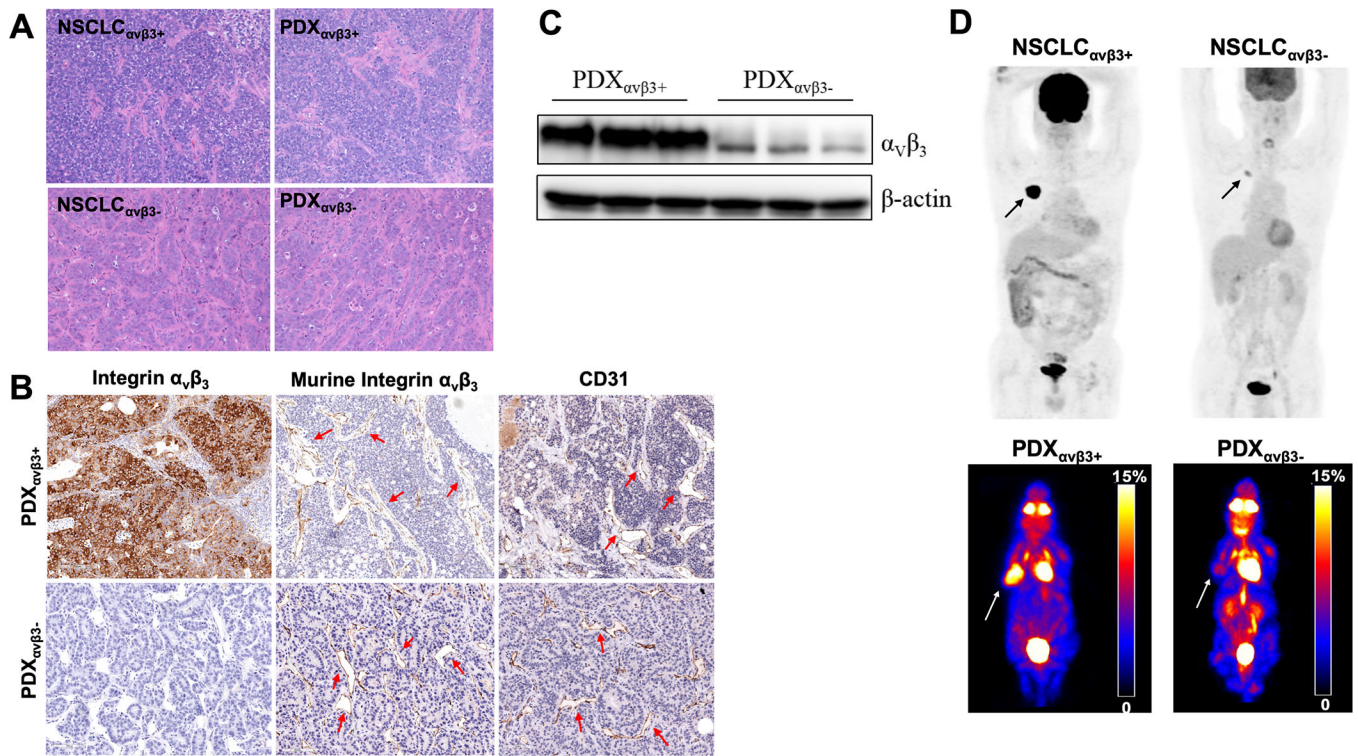
Fig. 1.
Histopathology and positron-emission tomography (PET) imaging of patient-derived xenografts (PDX) and parental tumours. (A) Haematoxylin and eosin (H&E) staining in human NSCLCs and corresponding PDXs; (B) Immunohistochemistry staining of integrin $\alpha_v\beta_3$ expression and CD31 in human NSCLCs and corresponding PDXs (tumour vasculatures were indicated by arrows); (C) The expression of integrin $\alpha_v\beta_3$ was detected by Western blot analysis; (D) ^{18}F-FDG PET imaging in two patients with NSCLC and corresponding PDXs.
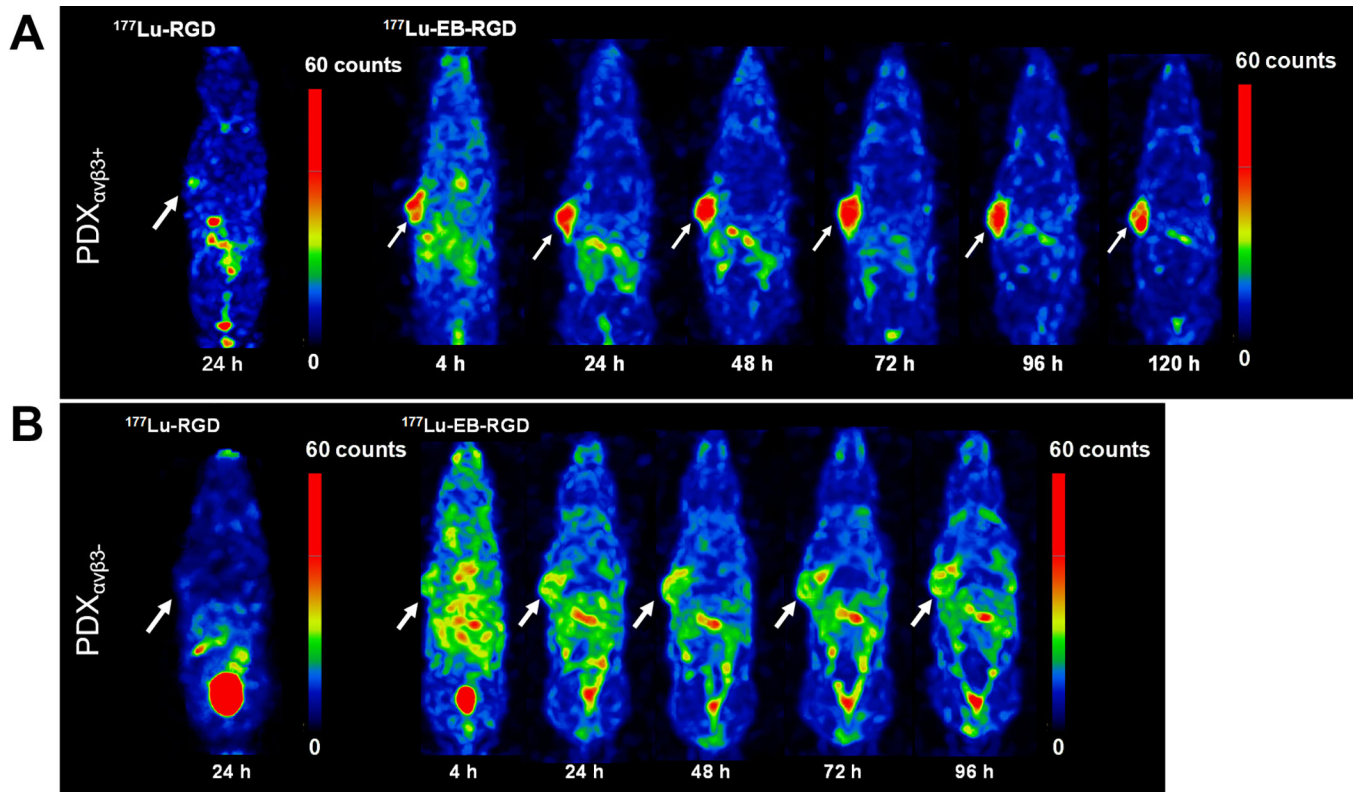
Fig. 2.
Maximum intensity projections from single-photon emission computer tomography (SPECT) imaging studies in PDXs. (A) Projection SPECT images of mice in PDX$_{\alpha v\beta3+}$ models at 24 h after 18.5 MBq ^{177}Lu-RGD injection (n = 4) and at 4, 24, 48, 72, 96 an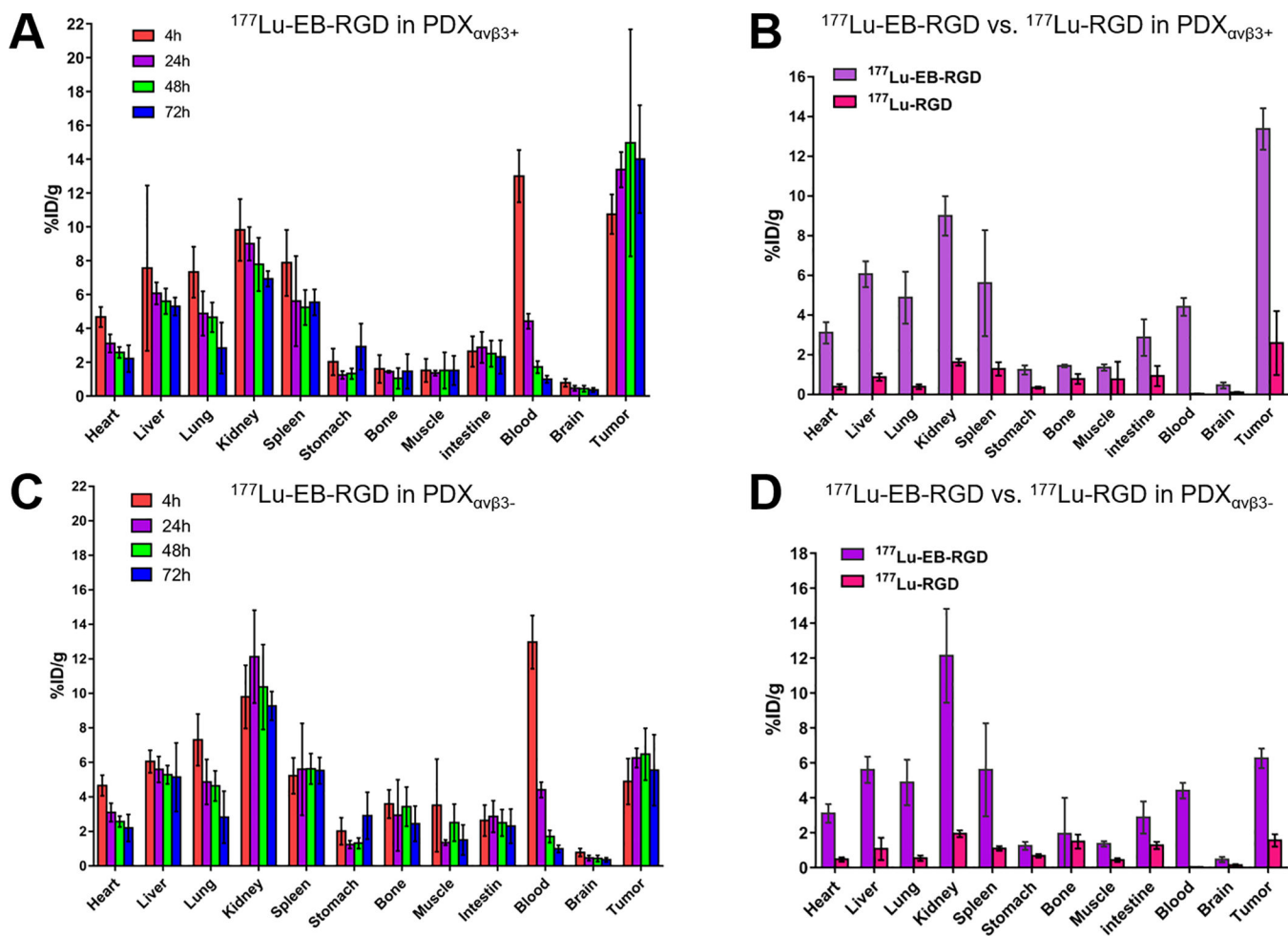d 120 h after 18.5 MBq ^{177}Lu-EB-RGD injection (n = 4). (B) Projection SPECT images of mice in PDX$_{\alpha v\beta3-}$ models at 24 h after 18.5 MBq ^{177}Lu-RGD injection (n = 4) and at 4, 24, 48, 72, and 96 h after 18.5 MBq ^{177}Lu-EB-RGD injection (n = 4).

Fig. 3.
Biodistribution of ^{177}Lu-EB-RGD in PDX groups. (A) PDX$_{\alpha v \beta 3+}$ models at 4, 24, 48 and 72 h post-injection (n = 3). (B) Comparison of ^{177}Lu-EB-RGD and ^{177}Lu-RGD in PDX$_{\alpha v \beta 3+}$ models at 24 h post-injection (n = 3/group). (C) ^{177}Lu-EB-RGD in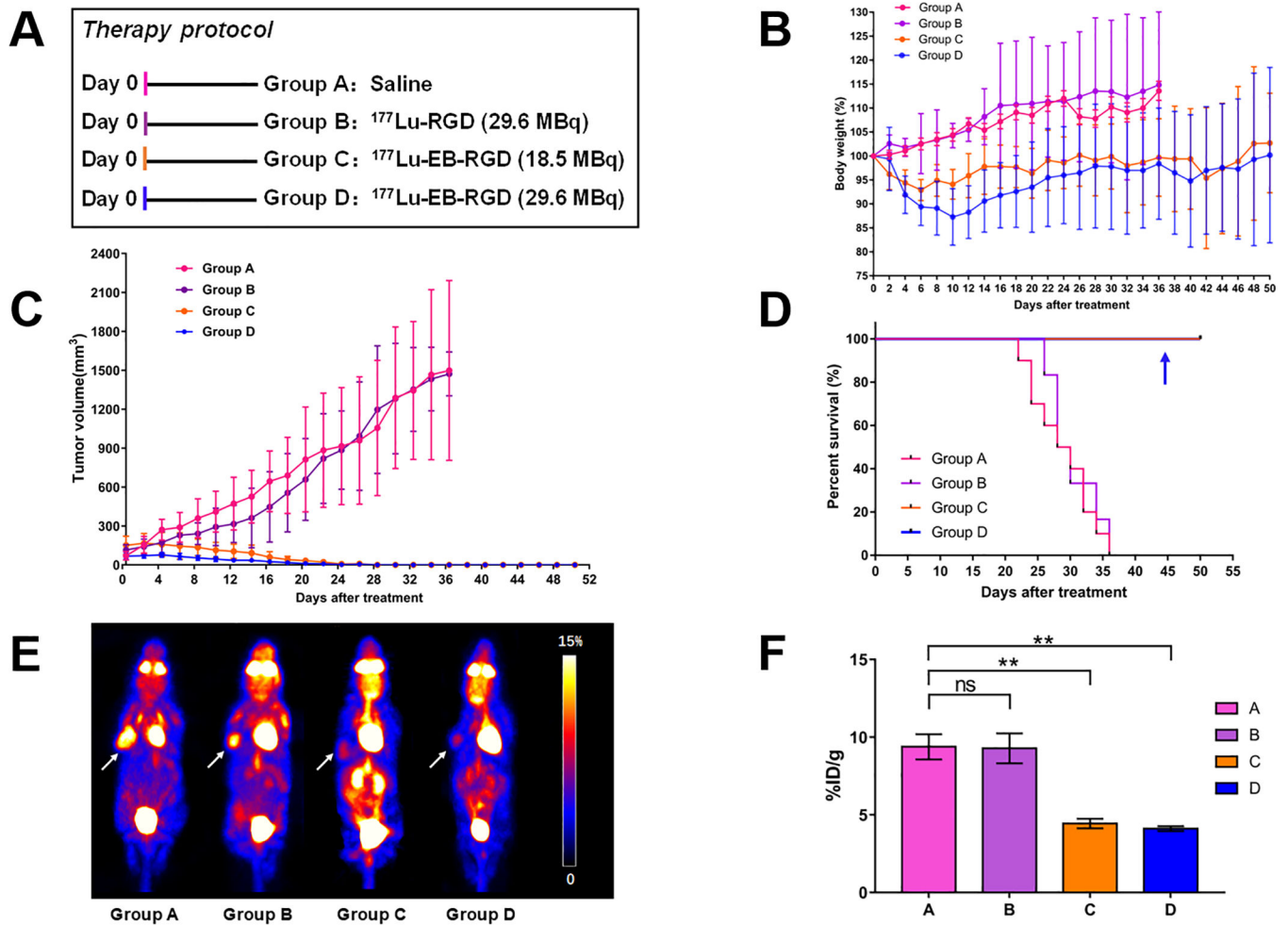 PDX$_{\alpha v \beta 3-}$ models at 4, 24, 48 and 72 h post-injection (n = 3/group). (D) Comparison of ^{177}Lu-EB-RGD and ^{177}Lu-RGD in PDX$_{\alpha v \beta 3-}$ models at 24 h post-injection (n = 3/group).

Fig. 4.

Therapy protocol and outcomes in $PDX_{\alpha v \beta 3+}$ mice. (A) Design of therapy protocol in $PDX_{\alpha v \beta 3+}$ models (n = 9 or 10 per group). (B) Change in body weight after treatment. (C) Change in tumour volume after treatment. (D) Survival of mice after therapy (Groups C and D were overlapped; Group D was indicated by the blue arrow). (E) Projection PET images of $PDX_{\alpha v \beta 3+}$ models injected with ^{18}F-FDG at 3 days after treatment. (F) PET quantification of the images in (E). ** P < 0.01
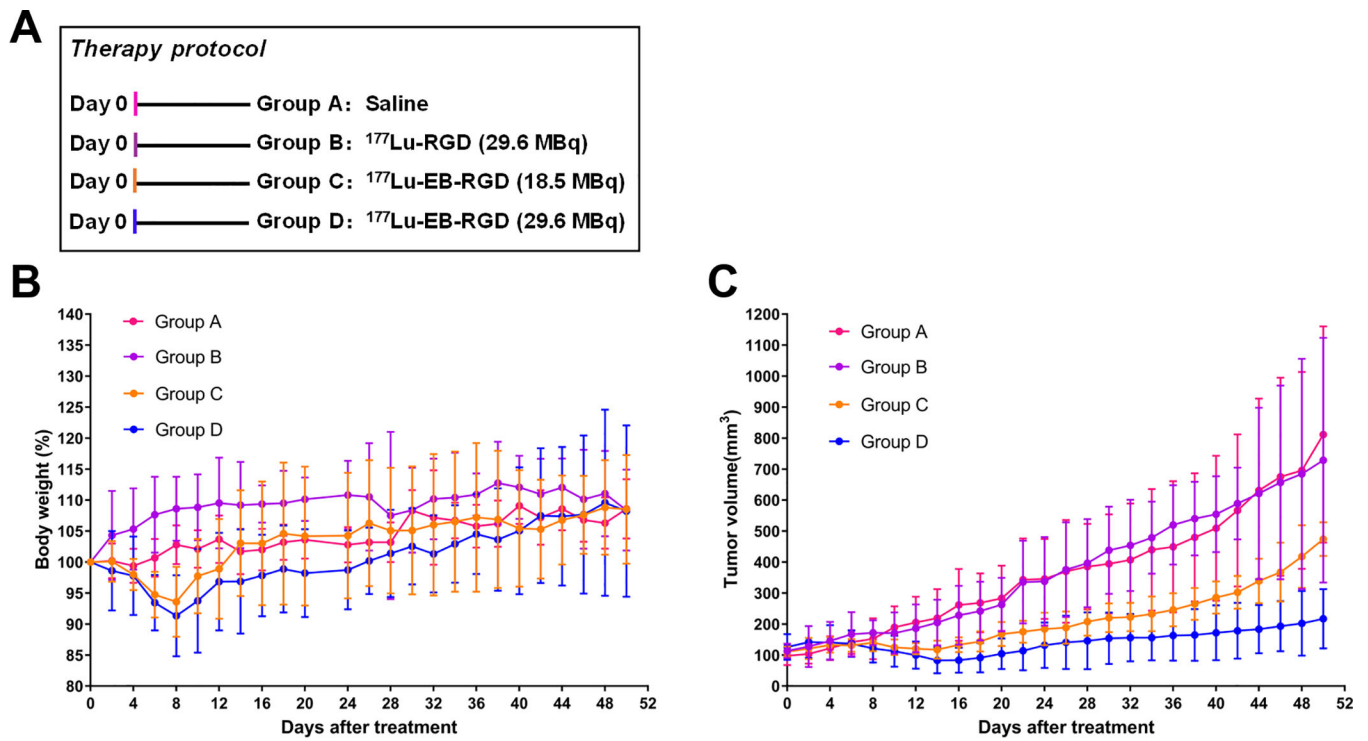
Fig. 5.

Therapy protocol and outcomes in $PDX_{\alpha v \beta 3-}$ mice (A) Design of therapy protocol in the NSCLC-PDXs with low integrin expression ($PDX_{\alpha v \beta 3-}$). (B) Change in body weight after treatment. (C) Change in tumour volume after treatment.
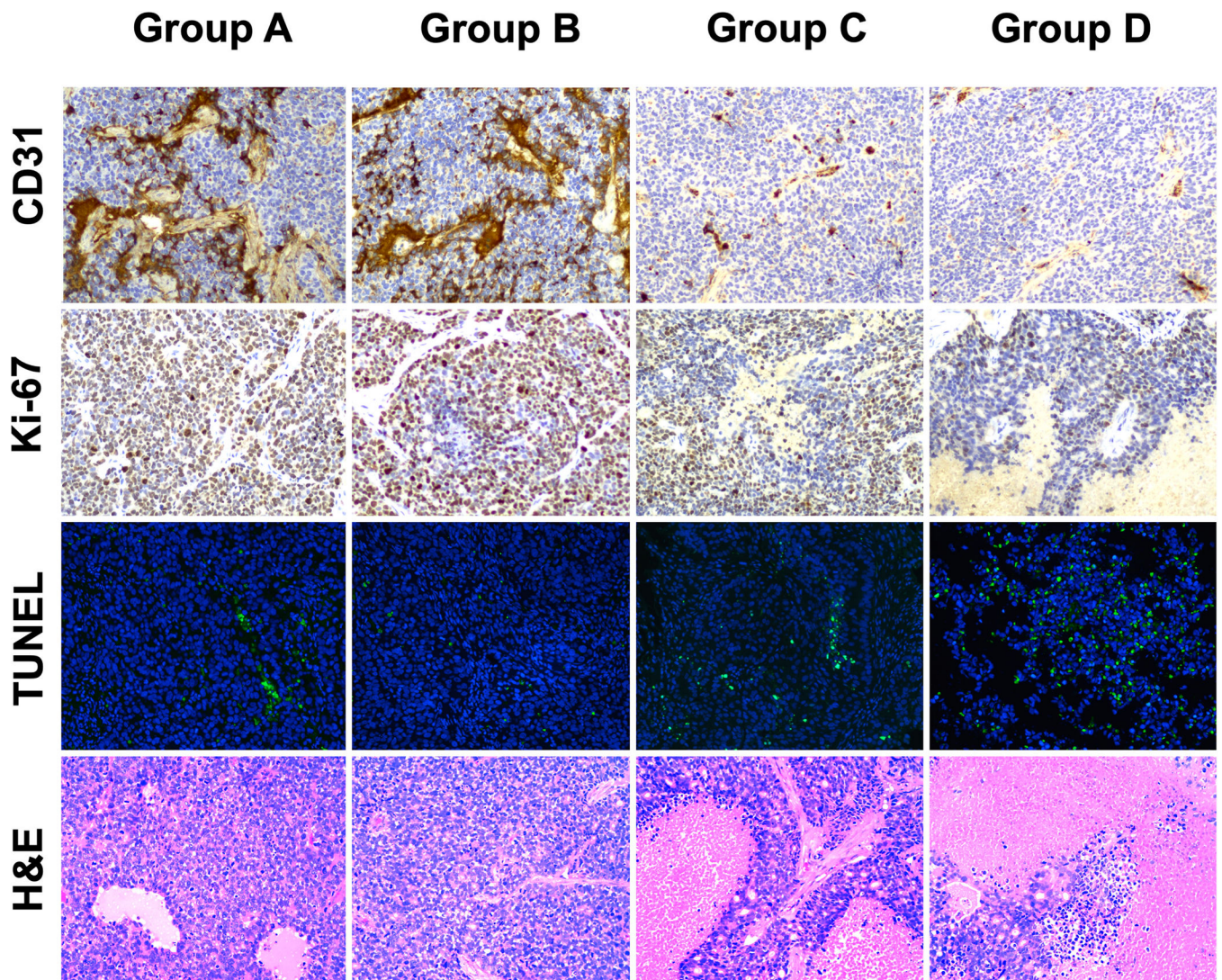
Fig. 6.

Immunohistochemistry (IHC) staining of excised tumours for CD31, Ki-67, TUNEL, and haematoxylin and eosin (H&E) after treatment with saline (group A), 29.6 MBq of ^{177}Lu-RGD (group B), 18.5 MBq of ^{177}Lu-EB-RGD (group C), and 29.6 MBq of ^{177}Lu-EB-RGD (group D) in PDX$_{\alpha v \beta 3+}$ models.